IRAQI BULLETIN OF GEOLOGY AND MINING (IBGM)\
IRAQ GEOLOGICAL SURVEY (GEOSURV-IRAQ)

*IBGM (**2025**, Vol 21; Issue 1)* *75-96*

LITHOLOGY AND GEOCHEMISTRY OF THE CHERT BEDS IN THE QULQULA RADIOLARIAN FORMATION FROM ZALAN AND KAOLOS SECTIONS NE-IRAQ

Sardar M. Ridha

Department of Geology, College of Science-Sulaimani University, e-mail: sardar.ridha@univsul.edu.iq

Type of the Paper (Article)
Received: 16/ 10/ 2024
Accepted: 18/ 11/ 2024
Available online: 27/ 06/ 20256

Abstract

Chert beds occur as thick successions of about 5 – 30 m thick in the middle part of the Qulqula Radiolarian Formation (ORF). They have studied geochemically in two sections for decoding the origin of silica, the provenance of clastic fraction, and the redox conditional environment. These successions are several and comprise about 25% thickness of the formation. For these purposes, 27 samples are quarried regularly from two exposed outcrop sections; Zalan and Kaolos in northeastern Iraq, located 20 Km north of Chwarta and 7 Km north of SaidSadik towns, respectively. These samples were analyzed for the major oxides, trace and rare earth elements, and total organic carbon. The thin section study indicated that most cherts have fine grain texture with ghosts of silicified detrital grains with few radiolarian tests. The discriminant function and binary diagrams of major oxides of samples indicated that these beds belong to the arc and diversional tectonic settings. The ratios of the trace elements indicate several origins of silica of QRF such as felsic and wind-blown detrital grains which are deposited under oxic to suboxic conditions and fairly biogenic. The discrimination diagrams and PAAS-normalized trace and rare earth elements indicate several sources of silica such as Mid-Oceanic-Ridge. High quantities of silica are released by sub-marine weathering and quartzose dust influx from the western desert as the primary source of silica. This condition is similar to the influx of silica-rich dust from the African Desert to the Amazon Forest. The radiolaria tests and sponges, whose siliceous remains are observed as a minor fraction of the silica in the bedded cherts. These sources supersaturated the environments QRF and developed bedded chert in deep basins below CCD where silica is stable instead of carbonates and falls within the range of felsic rock.

Keywords: Qulqula Formation; Chert Beds; felsic Provenance; Redox condition; Depositional environment.

ISSN 1811-4539, EISSN 3005-3714
https://doi.org/10.59150/ibgm2101a05
IBGM: http://ibgm-iq.org/
Academic Scientific Journals: www.iasj.net

1. Introduction

According to Buday (1980), the Qulqula Radiolarian Formation (QRF) (Jurassic Early Cretaceous) was defined by Bolton (1955), along Qulqula Gorge at the foothill of the Qandil mountain between Kozina and Baqiawa villages. He indicated its outcrop as a very thick sequence of bedded chert, siliceous shale, and cherty limestone. Buday (1980) explained that the lower and upper contacts of the formation are uncertain due to the intense deformation of the outcrop folding, faulting, and thrusting. Many authors such as (Aswad & Elias, 1988), (Jassim & Goff, 2006), (B. Al-Qayim et al., 2012), (Omar et al., 2015) and (Ali et al., 2017) mentioned the Qulqula Radiolarian Formation as a Group (Qulqula Group) based on the fact that the latter formation is overlaid by Qulqula Conglomerate Formation (Cenomanian). Recently (Baziany, 2014) studied it in detail QRF and divided it into several units, and indicated 24 thrust faults inside it.

This later formation was restudied by Karim & Baziany (2007) and Ghafor & Qadir (2009) based on stratigraphy and paleontology and confirmed that what was called the "Qulqula Conglomerate Formation" is a conglomerate of Eocene Red Bed Series. Based on this claimed conglomerate, (Lawa et al., 2013) proposed the development of an unconformity and a foreland basin at the end of Cenomanian, they called it the "Kurdistan Foreland Basin".

The Qulqula Radiolarian Formation has wide geographic distributions in Iraq and Iran, in the latter country it is known as Kermanshan Radiolarite. In Iraq, the main exposure is located in the north and northeast of Sulaimaniyiah Governorate, in an area known as the Sharbazer area between the Mawat and Khurmal towns.

The formation was deposited in the deep basin environment of southern Neo-Tethys in the trench and basin plain between Arabian and Iranian Plates below a carbonate compensation depth (CCD) thickness of about 2000 m. In Turkey, similar rocks known as the Celio Series and the continuation of Tanjero are considered to be Late Cretaceous – Paleocene (Altinli, 1966), while in northern Iran, the Radiolarite rocks known as Karaj Formation are aged Early and Middle Eocene (Darvishzadeh, 1992). In this area, the Qulqula Radiolarian Formation consists of bedded cherts of different colors, brown siliceous shale, marl, and limestones. These lithologies occur as thick bedded packages each one 10 – 30 thick. These lithologies repeated several times across the outcrop apparent thickness mainly due to folding and faulting. Therefore, the true thickness is not known, but it may be more than 1000 meters. Most lithologies of the formation are soft and thin-bedded except its limestone which is stiff and thick-bedded in some places. Therefore, the formation is located mainly inside low land between high mountain series along the Iraq – Iran Border.

Despite its tectonic and stratigraphic importance, there are few detailed studies on the formation, (Karim et al., 2009) studied the limestone succession of the lower part of the formation and proved tectonic repetition of succession four times. Al-Qayim et al. (2018) Aged the formation by radiolarian biozonation and inferred its deposition during the Middle Jurassic (Bajocian) to early Late Cretaceous (Late Cenomanian). Another new study is that of (Al-Sheraefy et al., 2022) who studied geochemistry, depositional environment, and provenance of

Formation in one section near Nal Parez town from the Penjween area. This study aims to explain the geochemistry of the bedded chert in the Zalan, and Kaolos sections (Figures 1, 2, 3, and 4), in addition to the the tectonic setting and provenance.

In Iraq and Iran, several tectonic and paleogeographic models are drawn for manifesting the depositional setting of the bedded cherts. In geologic literature, the QRF is considered the remnant sediment of the Neo-Tethys Ocean. Later (Karim H. K., 2024) and (Karim & Abioui, 2023) changed the Sanandaj-Sirian Zone to a deep basin as part of the Neo-Tethys Ocean and stated that QRF was deposited inside this zone which was deformed and sandwiched between the Arabian and Iranian Plates. During the Late Cretaceous, the QRF was uplifted as an accretionary prism forming terrestrial land which was the heart of the Zagros Mountain belt. In front of this land, a Zagros Foreland Basin was developed in which Shiranish and Tanjero Formations were deposited receiving detritus from the erosion of uplifted accretionary Prism.

2. Location and Geology of the Study Area

The studied area is located within Sulaimaniyah Governorate in Northeastern Iraq near the border with Iran (Figure 1). The formation is surveyed in the Sharbazer, Mawat, and Avroman areas for indication of the lithologies and stratigraphic relations (Baziany, 2014). In this study, two sections are sampled for geochemical analysis and petrographic study. The first one is located 3.3 Km northeast of Zalan village and called Zalan section (Figure 3) at latitudes 35°41'11.05" N and 45°43'23.40" E. This section represents the chert of the middle part of the Formation. The second section is located 1 Km northeast of the Kaolos village on the paved road between Sulaimanyiah city and Penjween town (Figure 4) at latitudes 35°28'53.33" N and longitude of 45°51'49.65" E which represents cherts of the succession of the lower part of the formation.

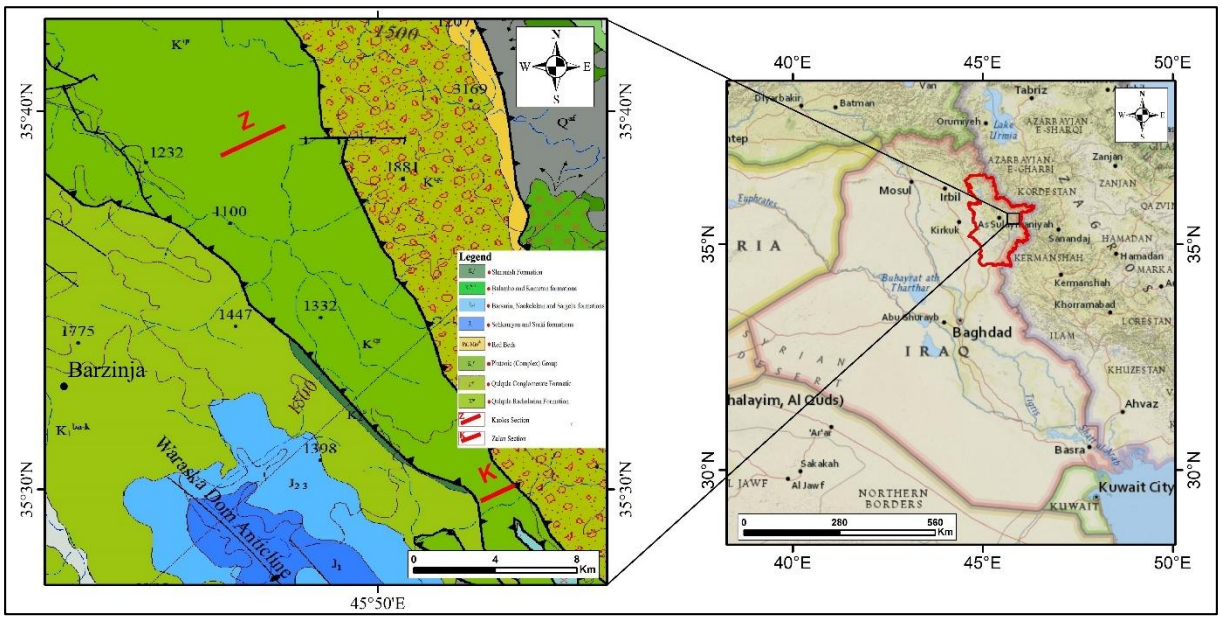

Figure 1. Location and geological map of the studied area (Sissakian & Fouad, 2014).

The outcrops of the formation have significant consequences on the geology of northern Iraq since the Main Zagros thrust Fault is indicated by Buday (1980) and (Jassim & Goff, 2006) at its southern limit of outcrops while the metamorphic and igneous rocks are located at its northern boundary (Figure 1). Highly fractured chert bed outcrops occupied the low land its limestone beds forming high mountains. The stratigraphic setting (boundary condition) of the QRF is not exactly clear, but field survey and published literature showed that it rested gradationally on the Avroman Formation (Triassic) which is observable in Avroman mountain near Khurmal, Ahmadwa, Biara, and Tawella villages (Figure 2). While in the Sharbazher and Mawat areas, its lower contact is tectonic with Balambo Formation, Red Bed Series.

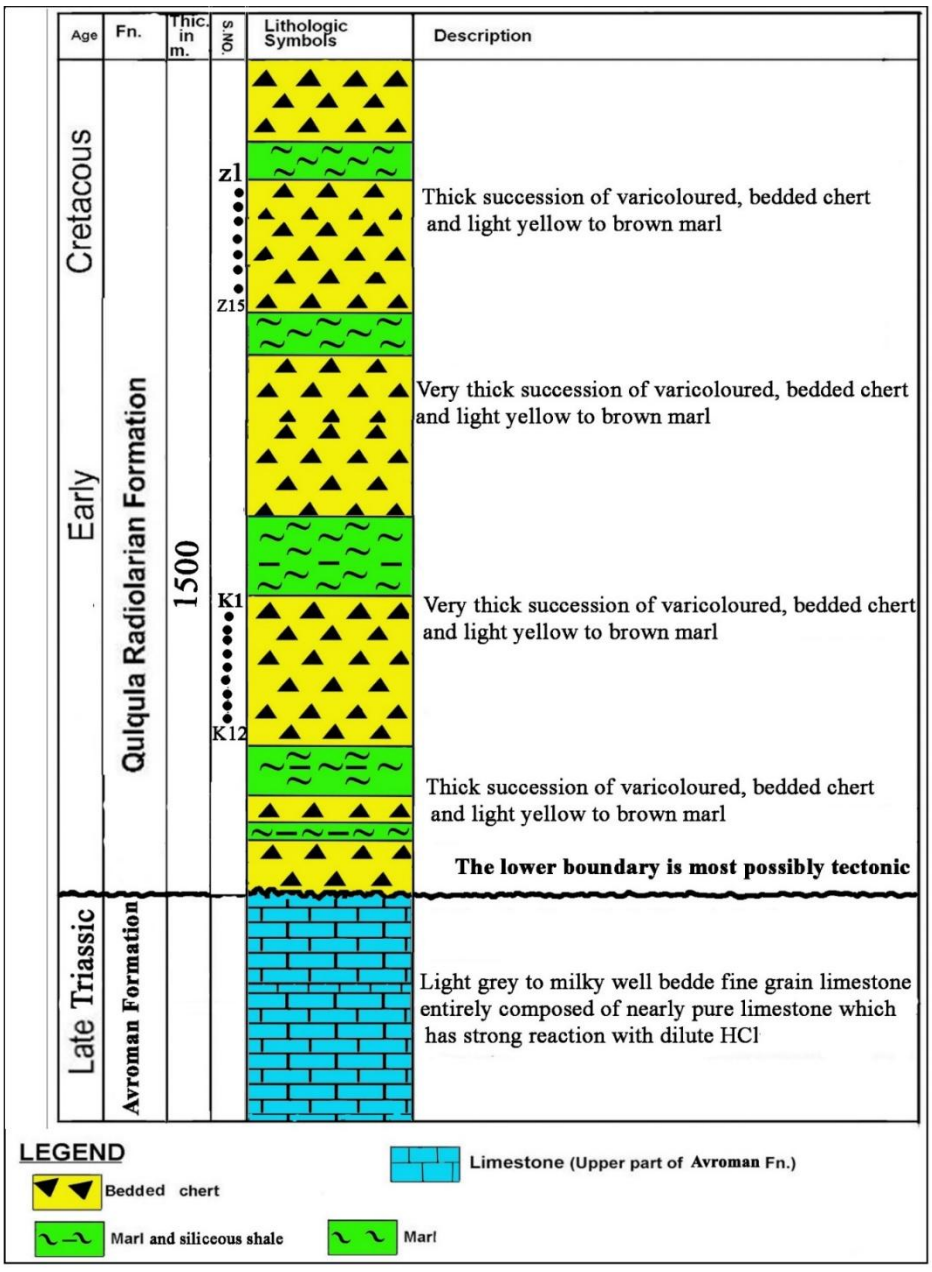

Figure 2. The general stratigraphic column of the studied area shows the location of the two sampled chert packages (Kaolos and Zalan sections) and the sample's location at the lower and upper part of the QRF.

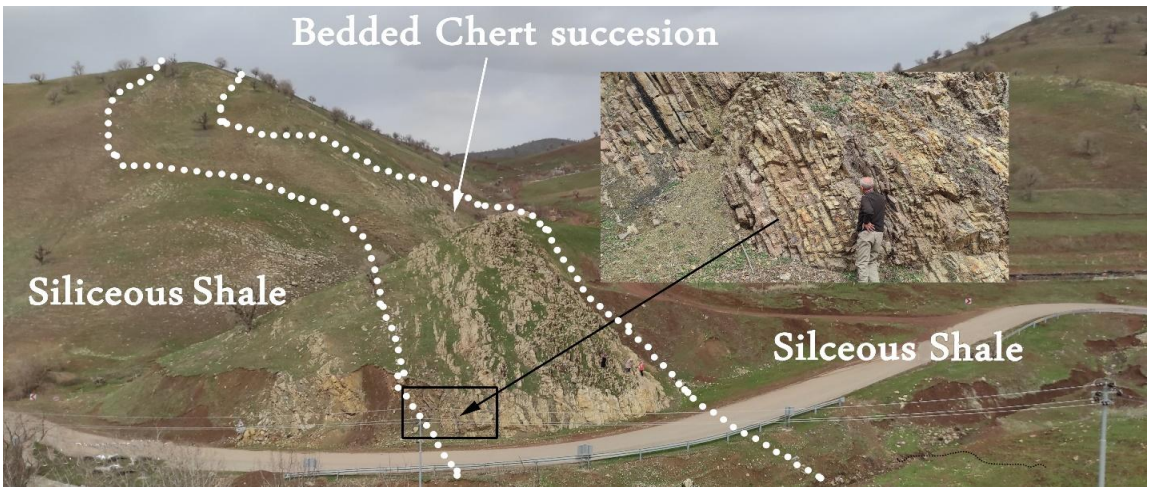

Figure 3. Zalan section at 3.3 Km northeast of (the Zalan village at latitudes 35°41'11.05" N and 45°43'23.40" E).

Figure 4. Kaolos section 1 Km northeast of the Kaolos village on the paved road between Sulaimanyiah city and Penjeen town, at latitudes 35°28'53.33"N and longitude of 45°51'49.65"E.

3. Materials and Methods

Twenty-seven chert 0.5 Km samples are collected from the two sections. Fifteen samples from Zalan and twelve from the Kaolos as described above (Figures 3 and 4) for geochemical and petrographical studies. From these samples, 20 thin sections are prepared at the University of Sulaimani/ Geology Department and studied under polarizer and stereoscopic microscopes. From these samples, a piece from each 27 samples is prepared for major oxides, LOI, and trace elements analyses. The fuse beads preparation and acid digestion are analyzed by using the inductively coupled plasma atomic emission spectrometry (ICP-AES). The trace elements were analyzed after four acid digestions by using inductively coupled plasma-mass spectrometry (ICP-MS) in Canada at the ALS International Laboratory.

4. Results

The chert beds of the QRF are composed mostly of chert and fine crystalline quartz, with streaks of varicolored, fine to cryptocrystalline chert. The beds are medium-hard and highly fractured.

4.1. The lithology of the formation

The lithology of the Qulqula Formation is highly variable and includes three end members, the first one is pure limestone and pure chert, passing through siliceous limestone. The chert beds are more common in the middle part. The second one is shale and marl and they grade to siliceous marl and shale which are more common in the upper part of the formation. Between Kaolos and Nalparez villages the lithology is ferruginous shale which grades to brown shelly Jasper. Mentioned that the limestone of the lower part of QRF consists of an alternation of more than four detrital limestone successions each about 25 m thick with thick intervals of bedded chert and shale. He added that the limestones are mainly distinctly bedded and shallow marine in origin (transported from shallow marine facies).

4.1.1. Field and Petrographic Observations

The bedded chert comprised more than 25% of the thickness of the QRF which occurs as several succession of 5 – 30 m thick. They have a light brown color and contain different color bedded cherts such as white, grey, black, green, brown, and red due to the content of impurities. Each succession occurs relatively as pure chert beds, but occasionally few successions host shaley or carbonaceous, ferruginous beds. The same difference in lithologies is observable under polarizer microscopes since there are laminated fine grain, medium grain, and coarse grain chert. The thin-section study indicated the prevalence of silicified detrital grains which appear as rounded white grains (Figures 5 and 6). The radiolarian tests are common and observable in the thin section and appear as two types of grains, the first is rounded tests of radiolaria which are replaced by calcite. Submarine currents may transport these tests; therefore, they lose their sculpture. The second type is those tests that have well-preserved minute microstructures such as with pores and spines and have brown color (Figures 5 and 6). These types of radiolarian tests comprised no more than 10% of the bulk of all types of tests and the author thinks that they were settled from the water column and not transported radiolarians. Studied these tests in the Nalparez area between SaidSadiq and Penjween towns.

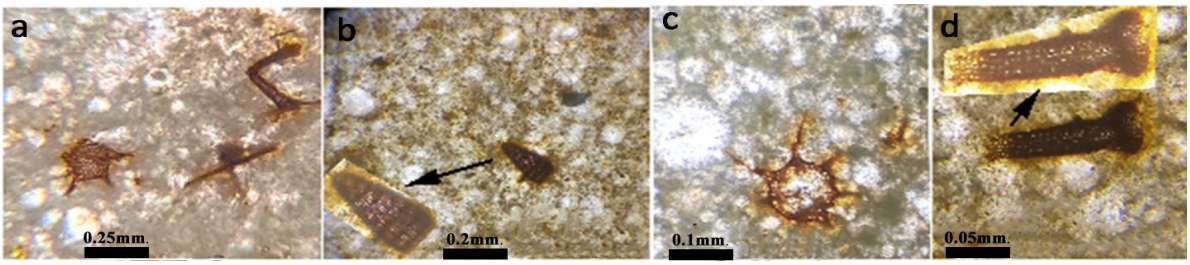

Figure 5 (a, b, c, d). Microphotographs under the polarized microscope of a bedded chert show oxidized radiolaria tests.

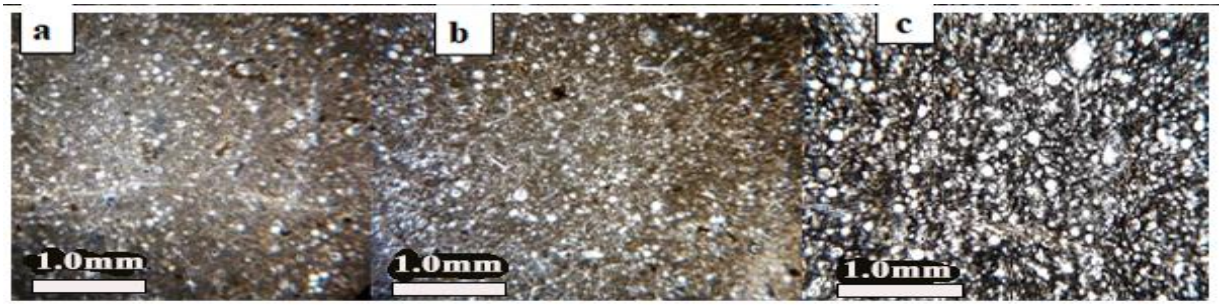

Figure 6. Microphotographs under the polarized microscope of Chert beds (partially recrystallized by quartz) in QRF, **a** and **b**) represent samples Q-1 and Q-10 from the Zalan section. XP light, **c**) represents samples K3 from the Kaolos section, Normal light, in both sections, is similar in petrographic properties.

4.2. Major Oxides

The major components of 27 bulk samples were analyzed for major oxide and elements from the two sections of Zalan and Kaolos. Table 1 shows the chert beds' major oxide concentrations and Loss on Ignition (LOI) in (wt.%). The range and average of the major oxide contents in Zalan section are: SiO_2 (89.1 to 97.9) % which is the most abundant oxide in the examined rocks (avg. 92.68%), Al_2O_3 (1.13 to 4.35) % (avg. 2.58%), Fe_2O_3 (1.22 to 3.37) % (avg. 2.16%) and LOI (0.9 to 2.66) %, (avg 1.89%). In the Kaolos section: SiO_2 (76.2 to 97.5) % which is the most abundant oxide in the examined rocks (avg. 93.01%), Al_2O_3 (0.95 to 3.05) % (avg. 1,84%), Fe_2O_3 (0.74 to 1.94) % (avg. 1.28%) and LOI (1.10 to 10.2) %, (avg 2.83%).

Low content of CaO and MgO is observed in all studied samples (avg. 0.82% and 0.58%) in the Zalan and Kaolse sections respectively. The average contents of Na_2O, K_2O, Cr_2O_3, TiO_2, MnO, and P_2O_5, are very low (< 0.5%) in all sections with a mild increase of K_2O in some samples of both sections as shown in Table 1, all the major oxide concentrations (except SiO_2) are lower than the Post Archean Australian Shale (PAAS).

4.3. Trace Elements

Table 2 shows the Chert beds trace element concentrations in (ppm). The range and average of the contents in Zalan section are Ba (29.1 to 101.5) ppm, (avg 50.91) ppm, Sr (34.3 to 60.8) ppm, (avg 44.05) ppm, Cr (20 to 60) ppm, (avg 31.3) ppm, Zr (15 to 56) ppm, (avg 33) ppm, Zn (13 to 49) ppm, (avg 26.1) ppm, Li (10 to 30) ppm, (avg 24) ppm, Cu (7 to 41) ppm, (avg 18.1) ppm, Ni (7 to 32) ppm, (avg 17.9) ppm, V (7 to 23) ppm, (avg 14.8) ppm, Rb (2.5 to 20.3) ppm, (avg 9.84) ppm, Nb (3 to 10.3) ppm, (avg 5.71) ppm, Y (1.6 to 7.6) ppm, (avg 4.41) ppm, Pb (2 to 9) ppm, (avg 4.27) ppm, Ga (2 to 6.4) ppm, (avg 3.92) ppm, Co (1 to 5) ppm, (avg 3.27) ppm, Mo (1 to 6) ppm, (avg 3.38) ppm, Sc (1 to 4) ppm, (avg 2.4) ppm, Ba (0.67 to 3.4) ppm, (avg 1.73) ppm. The average contents of C, S, Cs, Ta, and U are very low (< 0.5%) in all sections with mild increases of Hf in some samples of both sections. Trace element concentrations of the QRF are lower than that of PAAS, except Mo, which is slightly enriched. This depletion is clearly due to dilution by authigenic silica.

Table 1. Major Oxide percentages concentrations of the Chert beds, Qulqula Formation.

SN	SiO_2	Al_2O_3	Fe_2O_3	CaO	MgO	Na_2O	K_2O	Cr_2O_3	TiO_2	MnO	P_2O_5	1	2	3	4	LOI
Q1	92.6	1.23	1.22	1.99	0.43	0.04	0.09	0.003	0.04	0.01	0.01	0.50	30.8	0.94	100	2.44
Q2	92	1.86	1.72	1.67	0.55	0.07	0.14	0.005	0.07	0.01	0.01	0.52	26.6	0.93	100	2.46
Q3	91	2.62	1.98	1.45	0.67	0.04	0.34	0.002	0.12	0.01	0.04	0.57	21.8	0.92	98	2.66
Q4	94.2	2.2	1.62	0.24	0.54	0.11	0.34	0.005	0.09	0.02	0.02	0.58	24.4	0.95	98	1.45
Q5	92.9	3.04	2.17	0.23	0.97	0.06	0.38	0.005	0.10	0.01	0.03	0.58	30.4	0.93	99	1.83
Q6	92.4	2.42	2.4	0.22	1.04	0.05	0.20	0.003	0.10	0.01	0.03	0.50	24.2	0.93	99	1.66
Q7	92.1	2.68	2.69	0.16	0.91	0.05	0.22	0.006	0.09	0.02	0.02	0.50	29.8	0.93	99	1.74
Q8	94.3	2.7	2.06	0.11	0.71	0.05	0.37	0.006	0.07	0.01	0.01	0.57	38.6	0.94	98	1.43
Q9	89.1	4.35	3.37	0.17	1.37	0.1	0.56	0.003	0.19	0.03	0.02	0.56	22.9	0.9	94	2.5
Q10	94.2	2.13	2.19	0.12	0.71	0.04	0.18	0.006	0.09	0.01	0.01	0.49	23.7	0.94	100	1.31
Q11	89.3	3.96	2.62	0.17	1.03	0.13	0.52	0.006	0.17	0.03	0.03	0.60	23.3	0.91	94	2.23
Q12	94.7	1.73	1.39	0.22	0.27	0.07	0.21	0.003	0.10	0.01	0.01	0.55	17.3	0.96	100	2.17
Q13	91.6	3.44	2.78	0.12	1.09	0.09	0.45	0.006	0.14	0.03	0.03	0.55	24.6	0.92	98	1.85
Q14	91.9	3.22	2.82	0.08	1.28	0.09	0.32	0.005	0.12	0.04	0.01	0.53	26.8	0.92	98	1.76
Q15	97.9	1.13	1.3	0.09	0.1	0.06	0.16	0.003	0.04	0.01	0.01	0.47	28.3	0.97	100	0.9
Av	**92.7**	**2.581**	**2.16**	**0.47**	**0.78**	**0.07**	**0.30**	**0.004**	**0.10**	**0.02**	**0.02**	**0.5**	**22.8**	**0.93**	**98**	**1.89**
Max	**97.9**	**4.35**	**3.37**	**1.99**	**1.37**	**0.13**	**0.56**	**0.006**	**0.19**	**0.04**	**0.04**	**0.6**	**32.5**	**0.97**	**100**	**2.66**
Min	**89.1**	**1.13**	**1.22**	**0.08**	**0.10**	**0.04**	**0.09**	**0.002**	**0.04**	**0.01**	**0.01**	**0.5**	**13.9**	**0.9**	**94**	**0.9**
K1	90.3	3.05	1.94	0.35	0.90	0.09	0.45	0.003	0.16	0.01	0.07	0.61	19.1	0.93	97	2.81
K2	76.2	1.13	0.74	11	0.32	0.05	0.17	0.003	0.04	0.18	0.01	0.60	28.3	0.8	83	10.2
K3	92.8	2.95	1.41	0.33	0.65	0.09	0.54	0.002	0.14	0.01	0.03	0.68	21.1	0.94	100	2.71
K4	95.4	1.53	1.43	0.21	0.26	0.04	0.17	0.004	0.04	0.04	0.04	0.52	38.3	0.96	97	2.3
K5	94.6	0.98	1.13	0.33	0.16	0.05	0.15	0.005	0.04	0.01	0.01	0.46	24.5	0.97	98	1.42
K6	92.8	2.62	1.22	0.32	0.51	0.06	0.37	0.002	0.10	0.01	0.06	0.68	26.2	0.95	98	2.58
K7	95.3	2.01	1.19	0.25	0.35	0.07	0.30	0.004	0.09	0.01	0.05	0.63	22.3	0.95	100	2.2
K8	97.5	0.95	1.19	0.13	0.10	0.06	0.13	0.006	0.05	0.01	0.03	0.44	19	0.97	99	1.23
K9	95.3	1.7	1.12	0.23	0.32	0.04	0.23	0.002	0.07	0.01	0.04	0.60	24.3	0.96	97	2.5
K10	94	1.95	1.53	0.27	0.39	0.06	0.24	0.004	0.08	0.02	0.06	0.56	24.4	0.95	97	2.93
K11	95	2.03	1.45	0.25	0.43	0.07	0.31	0.003	0.09	0.01	0.05	0.58	22.6	0.95	98	1.92
K12	96.9	1.22	1.01	0.21	0.12	0.08	0.14	0.002	0.06	0.02	0.06	0.55	20.3	0.97	97	1.1
Av	**93**	**1.843**	**1.28**	**1.16**	**0.38**	**0.06**	**0.27**	**0.003**	**0.08**	**0.03**	**0.04**	**0.6**	**18.5**	**0.94**	**97**	**2.83**
Max	**97.5**	**3.05**	**1.94**	**11**	**0.90**	**0.09**	**0.54**	**0.01**	**0.16**	**0.18**	**0.07**	**0.7**	**35.8**	**0.97**	**100**	**10.2**
Min	**76.2**	**0.95**	**0.74**	**0.13**	**0.10**	**0.04**	**0.13**	**0.002**	**0.04**	**0.01**	**0.01**	**0.4**	**10.1**	**0.8**	**83**	**1.10**
PAAS	**62.80**	**18.90**	**7.22**	**2.20**	**1.30**	**0.11**	**3.70**		**1.0**	**0.11**	**0.16**					**6.0**

1 = $Al_2O_3/(Al_2O_3+Fe_2O_3)$; 2 = Fe_2O_3/TiO_2; 3 = Si/(Si+Al+Ca+Fe); 4 = Non-terrigenous Si%

Table 2. Trace elements concentrations in (ppm) of the Chert beds, Qulqula Formation.

S	C	Cr	Zr	Rb	Mo	Ni	Th	U	V	Co	Y	Sc	La	Zr/Sc	Th/Sc	Ni/Co	V/(V+Ni)	La/Sc	Mo/C	Cr/V	Y/Ni
Q1	0.44	20	15	2.5	2	8	0.67	0.63	7	2	1.6	1	2.7	15	0.67	4.00	0.47	2.7	4.55	2.86	0.20
Q2	0.38	30	19	4.1	2	11	1	0.22	14	3	2.5	1	3.2	19	1	3.67	0.56	3.2	5.26	2.14	0.23
Q3	0.32	20	37	10.4	<1	13	1.94	0.28	13	3	5.2	3	8.1	12.33	0.65	4.33	0.50	2.7	ND	1.54	0.40
Q4	0.08	60	29	10.5	4	12	1.43	0.24	11	2	3.9	2	6.4	14.5	0.72	6.00	0.48	3.2	50.00	5.45	0.33
Q5	0.05	30	32	12	3	20	1.8	0.38	16	4	5.2	3	7.8	10.67	0.6	5.00	0.44	2.6	60.00	1.88	0.26
Q6	0.07	20	29	6.6	<1	21	1.71	0.28	16	5	5.2	2	6.8	14.5	0.86	4.20	0.43	3.4	ND	1.25	0.25
Q7	0.04	40	31	7.5	5	23	1.67	0.64	14	4	4.4	3	5.4	10.33	0.56	5.75	0.38	1.8	125.00	2.86	0.19
Q8	0.03	40	37	10.6	4	21	1.45	0.29	10	3	3.8	2	8.7	18.5	0.73	7.00	0.32	4.35	133.33	4.00	0.18
Q9	0.06	20	56	20.3	1	32	3.4	0.35	22	5	7.6	4	13.1	14	0.85	6.40	0.41	3.28	16.67	0.91	0.24
Q10	0.05	40	26	5.6	5	14	1.39	0.22	13	3	2.9	2	4.2	13	0.70	4.67	0.48	2.1	100.00	3.08	0.21
Q11	0.04	40	52	17	3	24	2.77	0.32	17	4	6.7	4	10	13	0.69	6.00	0.41	2.5	75.00	2.35	0.28
Q12	0.6	20	33	7	6	14	1.61	0.24	23	2	4.2	2	6.7	16.5	0.81	7.00	0.62	3.35	10.00	0.87	0.30
Q13	0.05	40	42	16.5	4	27	2.37	0.27	19	4	5.4	3	8.6	14	0.79	6.75	0.41	2.87	80.00	2.11	0.20
Q14	0.16	30	36	12.3	3	21	2	0.24	18	4	4.8	3	8.2	12	0.67	5.25	0.46	2.73	18.75	1.67	0.23
Q15	0.18	20	17	4.7	2	7	0.71	0.14	9	1	2.8	1	2.7	17	0.71	7.00	0.56	2.7	11.11	2.22	0.40
Av	**0.17**	**31.33**	**32.73**	**9.84**	**3.38**	**17.9**	**1.73**	**0.32**	**14.8**	**9.84**	**14.29**	**1.73**	**0.32**	**14.8**	**4.41**	**5.53**	**0.46**	**2.90**	**53.05**	**2.35**	**0.26**
Max	**0.6**	**60.**	**56.**	**20.3**	**6.0**	**32.**	**3.4**	**0.64**	**23.**	**5.0**	**7.6**	**4.0**	**13.**	**19**	**1.0**	**7.0**	**0.62**	**4.35**	**133.33**	**5.45**	**0.4**
Min	**0.03**	**20.00**	**15.00**	**2.50**	**1.00**	**7.00**	**0.67**	**0.14**	**7.00**	**1.00**	**1.60**	**1.00**	**2.70**	**10.33**	**0.56**	**3.67**	**0.32**	**1.80**	**4.55**	**0.87**	**0.18**
K1	0.03	20	35	16.8	2	16	1.87	0.31	21	4	9.9	4	8.60	8.75	0.47	4.00	0.57	2.15	66.67	0.95	0.62
K2	2.58	20	12	5.6	2	5	0.53	0.5	19	1	6.8	1	5.90	12.00	0.53	5.00	0.79	5.9	0.78	1.05	1.36
K3	0.04	20	31	19.4	<1	11	2.52	0.31	21	2	6.9	4	8.60	7.75	0.63	5.50	0.66	2.15	ND	0.95	0.63
K4	0.65	40	10	4.6	6	16	0.72	0.15	21	6	6.7	2	5.30	5.00	0.36	2.67	0.57	2.65	9.23	1.90	0.42
K5	0.21	40	11	5.1	4	9	0.61	0.09	9	2	1.8	1	2.10	11.00	0.61	4.50	0.50	2.1	19.05	4.44	0.20
K6	0.04	20	23	12.4	1	13	1.47	0.31	20	2	7.3	3	5.90	7.67	0.49	6.50	0.61	1.97	25.00	1.00	0.56
K7	0.25	30	21	10	3	11	1.31	0.44	17	2	6.1	3	5.50	7.00	0.44	5.50	0.61	1.83	12.00	1.76	0.55
K8	0.35	40	12	3.5	5	10	0.65	0.15	9	1	3.4	1	2.80	12.00	0.65	10.00	0.47	2.8	14.29	4.44	0.34
K9	0.62	20	16	7.1	1	12	0.96	0.28	18	3	5.6	2	4.80	8.00	0.48	4.00	0.60	2.4	1.61	1.11	0.47
K10	0.9	30	21	7.8	3	17	1.21	0.25	30	3	8.2	3	6.50	7.00	0.40	5.67	0.64	2.17	3.33	1.00	0.48
K11	0.04	30	20	11	5	13	1.3	0.2	15	4	6.9	3	6.10	6.67	0.43	3.25	0.54	2.03	125.00	2.00	0.53
K12	0.03	20	13	4.2	2	5	0.91	0.47	21	3	6.4	1	5.80	13.00	0.91	1.67	0.81	5.8	66.67	0.95	1.28
Av	**0.48**	**27.5**	**18.75**	**8.96**	**3.09**	**11.5**	**1.17**	**0.29**	**18.42**	**2.75**	**6.33**	**2.33**	**5.66**	**8.82**	**0.53**	**4.85**	**0.61**	**2.83**	**31.24**	**1.80**	**0.62**
Max	**2.58**	**40**	**35**	**19.4**	**6**	**17**	**2.52**	**0.5**	**30**	**6**	**9.9**	**4**	**8.6**	**13**	**0.91**	**10**	**0.81**	**5.9**	**125**	**4.45**	**1.36**
Min	**0.03**	**20**	**10**	**3.5**	**1**	**5**	**0.53**	**0.09**	**9**	**1**	**1.8**	**1**	**2.1**	**5**	**0.36**	**1.67**	**0.48**	**1.83**	**0.78**	**0.95**	**0.2**
PAAS		**110**	**210**	**160**		**55**	**3.1**	**3.1**	**150**	**20**	**27**	**16**	**38.2**								

4.4. Rare Earth Elements

Table 3 shows the Chert beds REE concentrations in (ppm). The range and average LREE contents in Zalan section are: La (2.7 to 13) ppm, (avg 6.8 ppm), Ce (6.5 to 44) ppm, (avg 22 ppm), Pr (0.65 to 3.16) ppm, (avg 1.73 ppm), Nd (2.4 to 11.6) ppm, (avg 6.51 ppm), Sm (0.47 to 2.42) ppm, (avg 1.39 ppm), Eu (0.13 to 0.47) ppm, (avg 0.29 ppm) and Gd (0.48 – 1.95), (avg 1.18). In Kaolos section are: La (2.1 to 8.6) ppm, (avg 5.66 ppm), Ce (6.5 to 44) ppm, (avg 11.14 ppm), Pr (0.59 to 2.44) ppm, (avg 1.46 ppm), Nd (3.1 to 9.7) ppm, (avg 5.64 ppm), Sm (0.42 to 2.15) ppm, (avg 1.2 ppm), Eu (0.09 to 0.44) ppm, (avg 0.27 ppm) and Gd (0.35 – 1.8), (avg 1.13). The range and average HREE contents in Zalan section are: Ho (0.06 to 0.29) ppm, (avg 0.17 ppm), Er (0.17 to 0.79) ppm, (avg 0.46 ppm), Tb (0.06 to 0.3) ppm, (avg 0.17 ppm), Dy (0.32 to 1.61) ppm, (avg 0.9 ppm), Tm (0.02 to 0.1) ppm, (avg 0.06 ppm), Yb (0.14 to 0.8)

ppm, (avg 0.42 ppm) and Lu (0.02 – 0.11), (avg 0.06). In Kaolos section are: Ho (0.06 to 0.29) ppm, (avg 0.20 ppm), Er (0.17 to 0.79) ppm, (avg 0.54 ppm), Tb (0.06 to 0.28) ppm, (avg 0.17 ppm), Dy (0.32 to 1.62) ppm, (avg 1.0 ppm), Tm (0.02 to 0.1) ppm, (avg 0.08 ppm), Yb (0.14 to 0.8) ppm, (avg 0.46 ppm) and Lu (0.03 – 01), (avg 0.07). Generally, in both sections, all REE data normalized by PAAS are lower and show apparent positive Eu and Ce anomalies (Figure 7a and b). This was due to a strong influence of hydrothermal fluids on their precipitation (Douville et al., 1999). Although detrital feldspar minerals can also lead to positive Eu anomalies (Owen et al., 1999), the absence of correlation of Eu anomalies with Al_2O_3 contents indicates that aluminosilicate minerals, such as feldspar, did not contribute to the positive Eu anomalies (Kato & Nakamura, 2003).

Table 3. Rare Earth Elements concentrations in (ppm) of the Chert beds, Qulqula Formation.

SN	La	Ce	Pr	Nd	Sm	Eu	Gd	Ho	Er	Tb	Dy	Tm	Yb	Lu
	(ppm)													
Q1	2.7	6.5	0.65	2.4	0.47	0.13	0.48	0.06	0.17	0.06	0.32	0.02	0.14	0.02
Q2	3.2	8.8	0.8	3.1	0.67	0.17	0.54	0.1	0.28	0.08	0.49	0.03	0.21	0.04
Q3	8.1	25.8	2.03	7.6	1.56	0.3	1.35	0.19	0.53	0.18	0.98	0.08	0.44	0.07
Q4	6.4	20.8	1.55	5.9	1.24	0.3	0.98	0.16	0.42	0.14	0.77	0.05	0.37	0.06
Q5	7.8	27.6	2.24	8.6	1.92	0.37	1.51	0.2	0.46	0.21	1.02	0.07	0.47	0.07
Q6	6.8	22.8	1.76	6.8	1.38	0.33	1.22	0.19	0.53	0.19	1.03	0.07	0.43	0.07
Q7	5.4	14.5	1.36	5.1	1.33	0.28	1.18	0.17	0.46	0.18	0.95	0.06	0.43	0.07
Q8	8.7	29.2	2.39	9	1.82	0.32	1.35	0.16	0.39	0.18	0.89	0.05	0.36	0.05
Q9	13.1	44	3.16	11.6	2.41	0.47	1.95	0.29	0.79	0.3	1.61	0.1	0.8	0.11
Q10	4.2	12.3	0.98	3.5	0.76	0.16	0.64	0.1	0.35	0.1	0.57	0.05	0.29	0.05
Q11	10	32.6	2.61	9.8	2.16	0.4	1.93	0.27	0.71	0.29	1.43	0.1	0.66	0.1
Q12	6.7	21.1	1.65	6	1.34	0.28	1.15	0.14	0.46	0.17	0.87	0.06	0.47	0.06
Q13	8.6	30.5	2.16	8	1.7	0.34	1.5	0.2	0.59	0.21	1.14	0.08	0.6	0.09
Q14	8.2	28.4	2	7.5	1.52	0.32	1.3	0.18	0.53	0.19	1.01	0.07	0.47	0.06
Q15	2.7	7.5	0.65	2.7	0.57	0.17	0.6	0.08	0.26	0.09	0.48	0.03	0.19	0.04
Av	**6.84**	**22.16**	**1.73**	**6.51**	**1.39**	**0.29**	**1.18**	**0.17**	**0.46**	**0.17**	**0.90**	**0.06**	**0.42**	**0.06**
Max	**13.1**	**44**	**3.16**	**11.6**	**2.41**	**0.47**	**1.95**	**0.29**	**0.79**	**0.3**	**1.61**	**0.1**	**0.8**	**0.11**
Min	**2.7**	**6.5**	**0.65**	**2.4**	**0.47**	**0.13**	**0.48**	**0.06**	**0.17**	**0.06**	**0.32**	**0.02**	**0.14**	**0.02**
K1	8.6	22.8	2.44	9.7	2.15	0.44	1.8	0.32	0.85	0.28	1.62	0.12	0.74	0.1
K2	5.9	8.7	1.13	4	0.85	0.2	0.85	0.18	0.55	0.15	0.9	0.09	0.53	0.08
K3	8.6	18.5	2.16	8	1.64	0.35	1.4	0.24	0.63	0.21	1.21	0.1	0.55	0.08
K4	5.3	8.1	1.53	6.2	1.4	0.31	1.32	0.22	0.62	0.18	1.09	0.07	0.4	0.06
K5	2.1	4.7	0.59	2.2	0.42	0.09	0.35	0.06	0.17	0.06	0.32	0.03	0.14	0.03
K6	5.9	11.9	1.56	6.1	1.3	0.29	1.23	0.24	0.65	0.19	1.13	0.08	0.49	0.08
K7	5.5	11.2	1.41	5.6	1.2	0.28	1.19	0.2	0.52	0.17	0.96	0.07	0.51	0.08
K8	2.8	5.9	0.82	3.1	0.66	0.14	0.64	0.11	0.33	0.09	0.57	0.04	0.25	0.04
K9	4.8	8.2	1.14	4.6	1.03	0.2	0.9	0.17	0.45	0.13	0.85	0.06	0.4	0.06
K10	6.5	10.1	1.76	6.7	1.42	0.35	1.44	0.25	0.66	0.23	1.33	0.1	0.63	0.08
K11	6.1	12.8	1.6	6.2	1.36	0.3	1.26	0.22	0.52	0.19	1.04	0.07	0.44	0.07
K12	5.8	10.8	1.35	5.3	1.13	0.24	1.12	0.19	0.49	0.16	1.02	0.07	0.44	0.06
Av	**5.66**	**11.14**	**1.46**	**5.64**	**1.21**	**0.27**	**1.13**	**0.20**	**0.54**	**0.17**	**1.00**	**0.08**	**0.46**	**0.07**
Max	**8.6**	**22.8**	**2.44**	**9.7**	**2.15**	**0.44**	**1.8**	**0.32**	**0.85**	**0.28**	**1.62**	**0.12**	**0.74**	**0.1**
Min	**2.1**	**4.7**	**0.59**	**2.2**	**0.42**	**0.09**	**0.35**	**0.06**	**0.17**	**0.06**	**0.32**	**0.03**	**0.14**	**0.03**

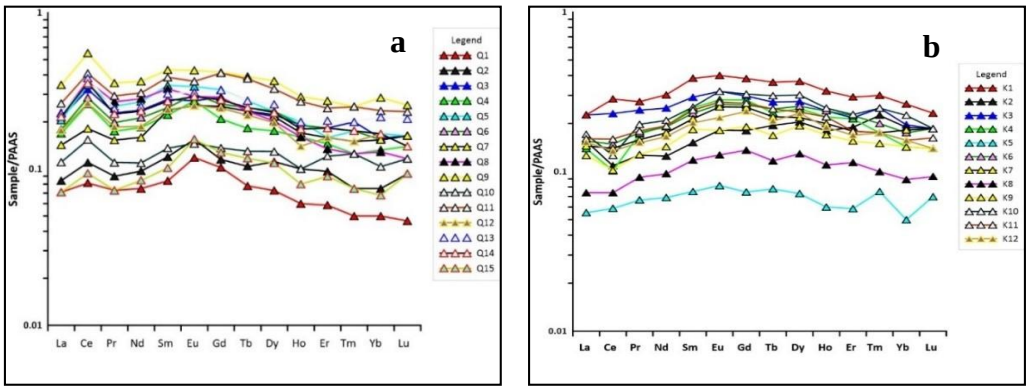

Figure 7. Post-Archean Australian Shale (PAAS) normalized REE patterns for, a) Zalan samples, and b) Kaols samples. The PAAS normalizing factors are from (Taylor & McLennan, 1985).

The REE values in ppm have been normalized by Chondrite. The results in both sections are higher than the chondrite. The low rare earth elements (LREE) concentrations are much higher than those of high rare earth elements (HREE; Figure 8a and b), which suggests that little plagioclase fractionation took place (Cullers & Graf, 1984). The negative Eu anomaly is found in most sample rocks of both sections. This indicates shallow differentiation of plagioclase formation.

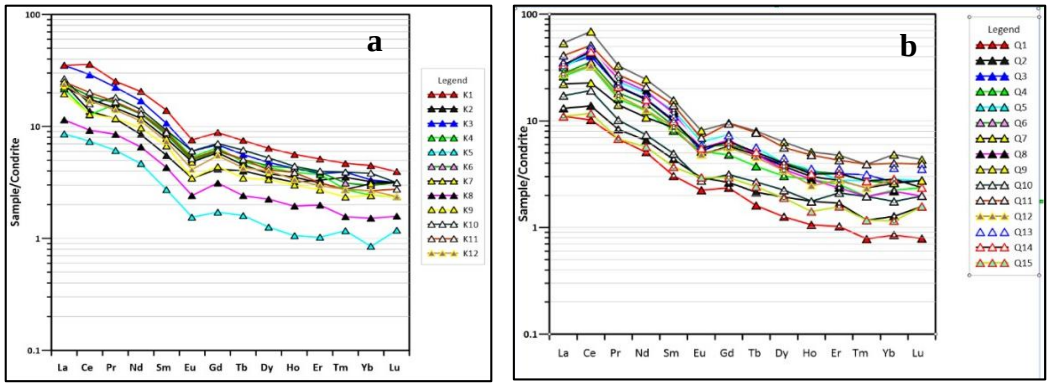

Figure 8. Chondrite-normalized (Evensen et al., 1978), REE plot of bedded cherts showing steep patterns, and it can be seen similar for both sections with only a small negative Eu abnormal, a) Zalan, b) Kaolos.

5. Discussion

5.1. Provenance

Ti and Al are immobile elements and they are considered clastic input indicators, whereas Fe-enrichment is considered an indicator for hydrothermal fluid precipitation (Fu et al., 2015). Therefore, the Fe/TiO_2 and $Al_2O_3/(Al_2O_3+Fe_2O_3)$ ratios are reliable indicators for characterizing the sedimentary setting (. Qulaqula Formation has an $Al_2O_3/(Al_2O_3+Fe_2O_3)$ ratio between 0.44 and 0.72 (average 0.6); and a Fe_2O_3/TiO_2 ratio between 10.1 and 32.5 (average

18.5) (Table 1). On the Fe/TiO_2 versus $Al_2O_3/(Al_2O_3+Fe_2O_3)$ diagram, it is evident that all samples are located in the deep ocean field (Figure 9). These values indicate that the Qulaqula Formation is slightly affected by terrigenous clastic input.

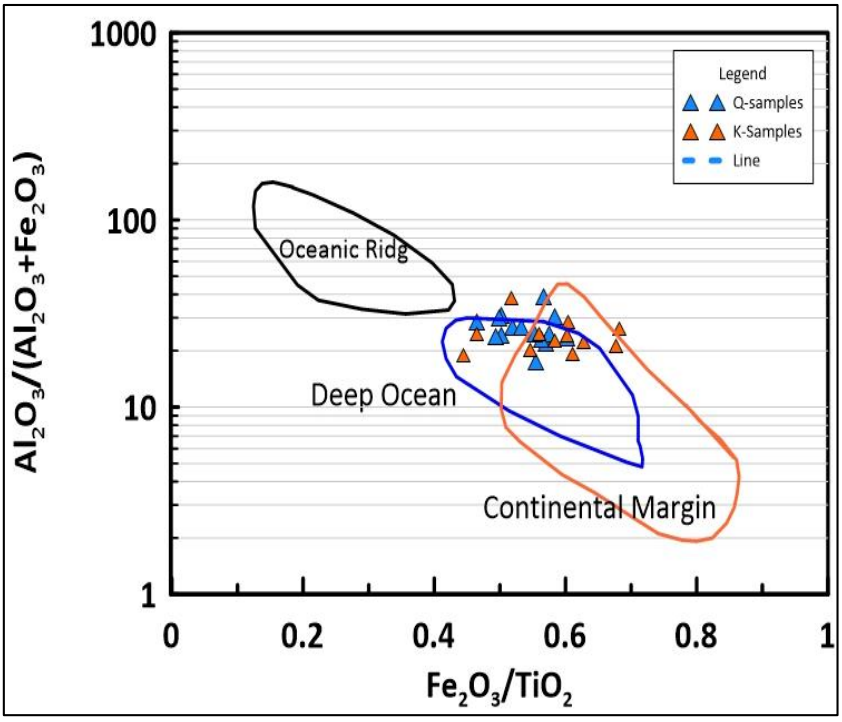

Figure 9. Identification of sedimentary setting based on $Al_2O_3/ (Al_2O_3+Fe_2O_3)$ versus Fe_2O_3/TiO_2 (Murray, 1994).

According to Pearce et al. (1984), Yb vs Ta diagram the studied samples belong to vol arc granites (Figure 10). Recycling of clastic rocks will lead to heavy minerals enrichment, such as zircon (Ma et al., 2015). Therefore, the Th/Sc and Zr/Sc ratios are widely used to deduce the sedimentary recycling degree (McLennan et al., 1993); (Al-Maadhidi et al., 2023). The Th/Sc and Zr/Sc ratios of the studied samples of the Qulqula Formation are between 0.36-1.0 and 5-19, respectively. Figure 11 shows no sedimentary recycling of the Qulaqula Formation chert beds and the chemical composition represents the original composition. These rocks are derived from felsic rocks. The addition of authigenic (biogenic) silica affects some ratios used for the interpretation of provenance and tectonic settings, such as the SiO_2/Al_2O_3 ratio. The K_2O/Rb and Yb/Ta are used to assess the volcanic and volcanic arc contribution to rock composition and source. The high values of K_2O/Rb in studied samples indicate the low effect of weathering (Figures 10 and 12), (McLennan et al., 1990); (Ran et al., 2015). All the studied samples of the Qulqula Formation have K_2O/Rb ratios typical of sediments generated from the upper continental crust (UCC). Still, they are diluted by silica of biogenic origin (as seen below). They have low values of K_2O and Rb relative to PAAS, but the ratio is similar; therefore, they are located in the same line (Figure 12). To support this interpretation, the Cr/V and Y/Ni ratios were used to infer the provenance (Figure 13). As shown in that figure, most of the samples are close to the PAAS area but lower in concentration; supporting felsic provenance. Th-La-Sc and

V-Ni-Th ternary diagrams also support the felsic provenance of the sediments, and most of the samples are also located close to PAAS (Figures 15 and 16). The PAAS normalized REE patterns are lower for the two studied sections of Zalan and Kaolos (Figure 7a and b). The chondrite-normalized REE patterns have negative Eu anomaly; supporting the felsic provenance (Figure 8a and b).

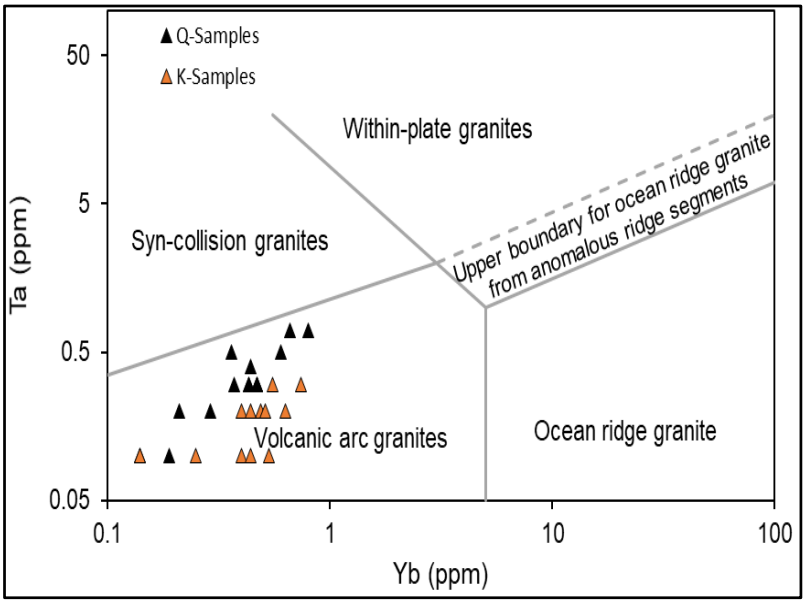

Figure 10. Yb vs Ta Discr within-plate granites, vol arc granites-ocean ridge granites (Pearce et al., 1984).

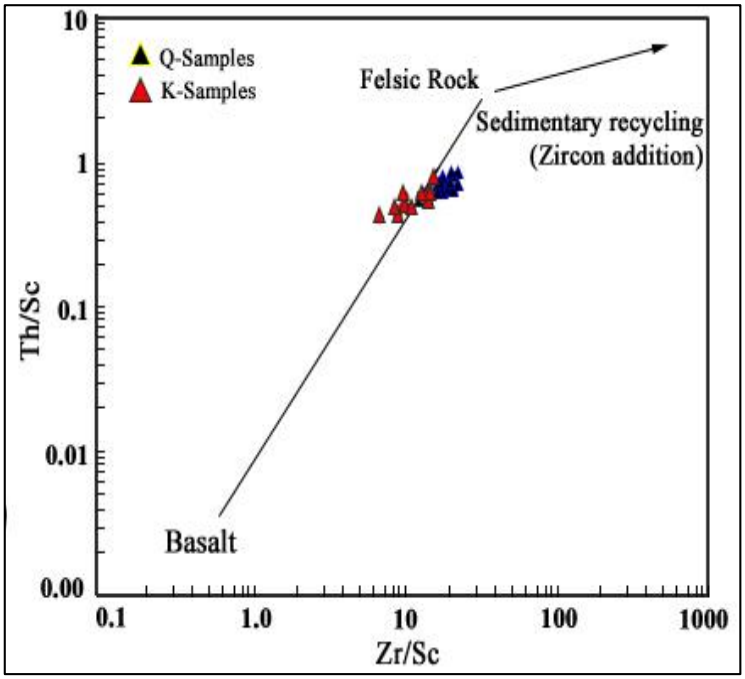

Figure 11. Recycling of sediments of chert samples from Qulqula Formation (McLennan et al., 1990).

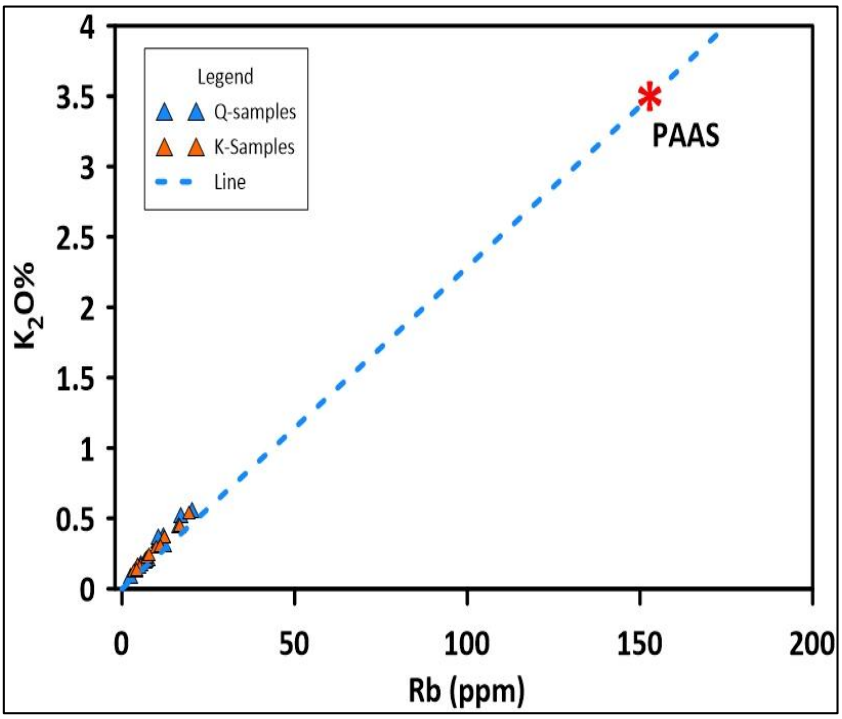

Figure 12. K_2O versus Rb diagram of chert samples from the Qulqula Formation shows that these samples are not affected by contribution from volcanoclastic sediments nor by weathering (McLennan et al., 1990).

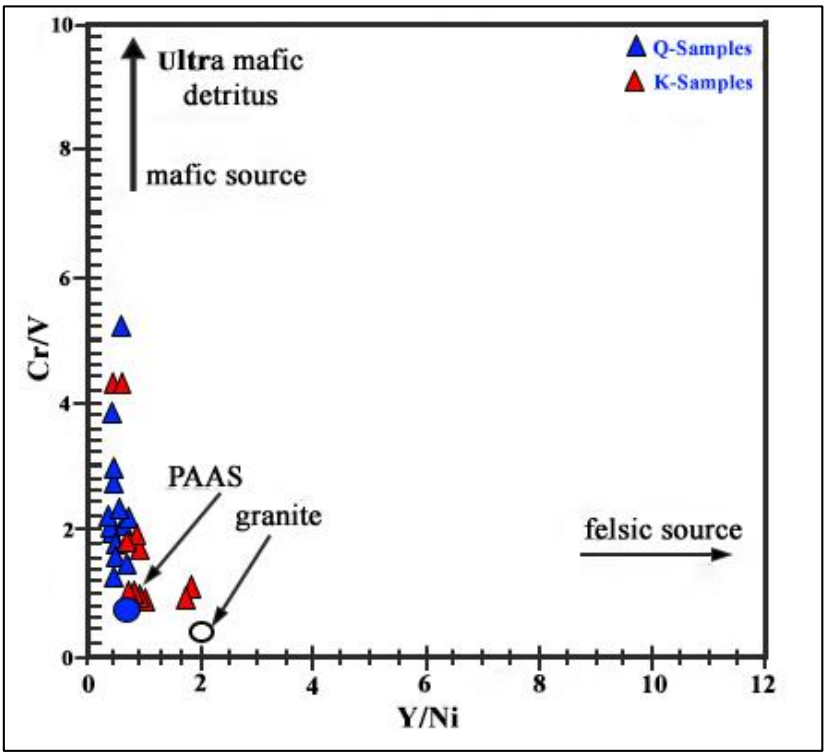

Figure 13. Identification of provenance of chert bed sediments based on Y/Ni versus Cr/V ratios (After (Mateen et al., 2022).

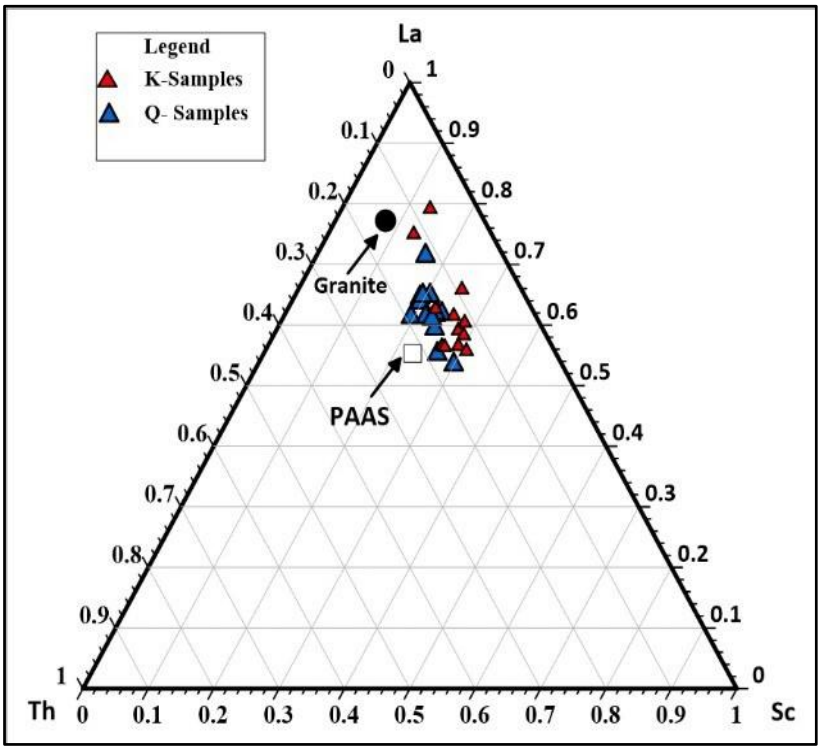

Figure 14. Identification of provenance of sediments of chert bed sediments based on Th-La-Sc ternary diagram (Taylor & McLennan, 1985).

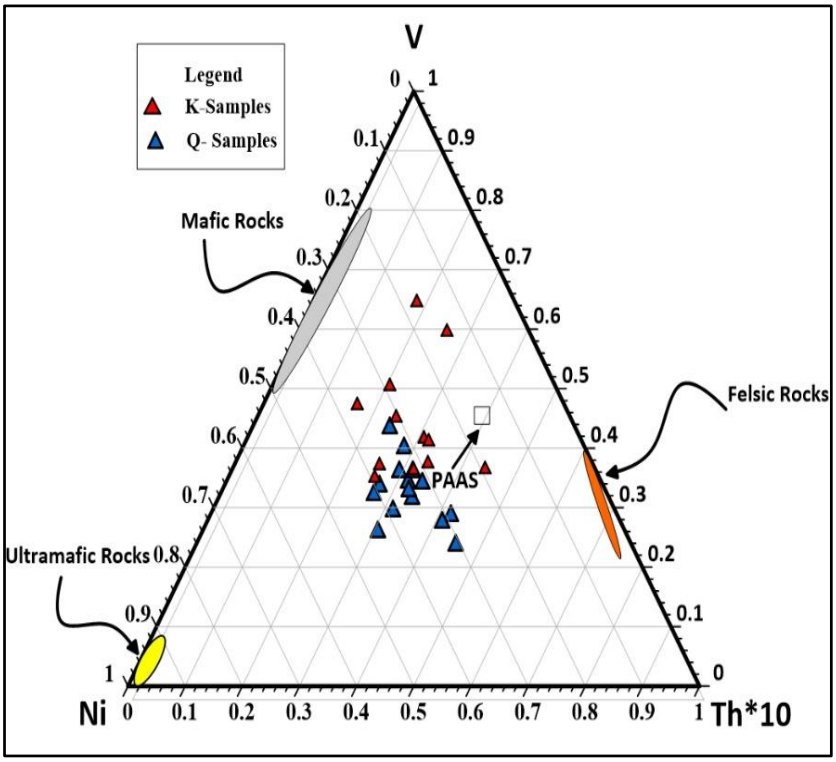

Figure 15. Identification of provenance sediments of chert bed sediments based on Ni-V-Th ternary diagram, after Post Archean Australian shale (PAAS) values are from (Taylor & McLennan, 1985).

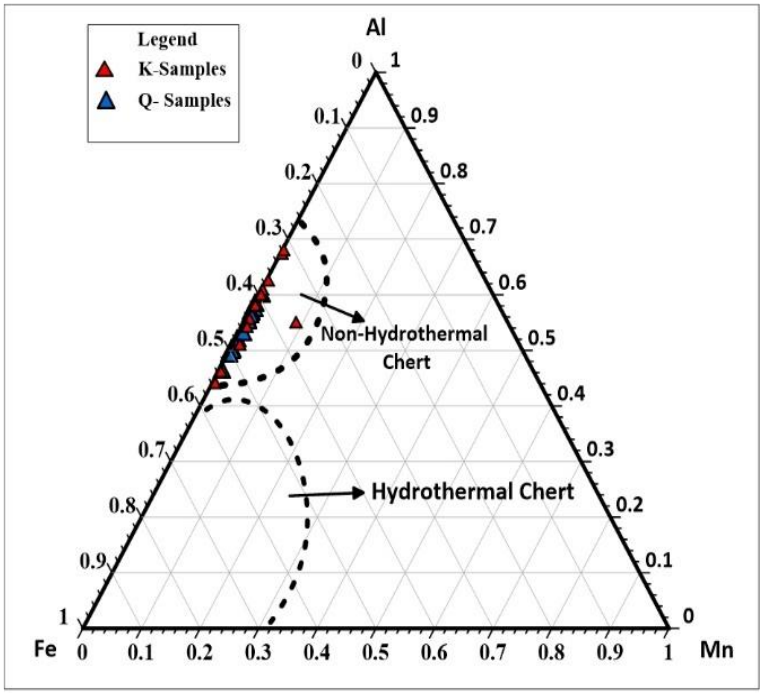

Figure 16. Fe-Al-Mn plot of Qulqula Formation showing the hydrothermal and non-hydrothermal cherts, (Adachi et al., 1986).

5.2. Origin of Silica

Many processes such as different sources, sediment input, sorting, and transporting, influence the geochemical characteristics of cherts (Ran et al., 2015). Generally, the silica in mud rocks has different sources; these are detrital silica (feldspar, clay, and quartz) transported from the continent by rivers; silica precipitated during diagenesis of clay minerals; hydrothermal fluids, and biogenic silica (Tatzel et al., 2017); (Gao et al., 2021); (LaGrange et al., 2020). For determination of the origin of chert and its geotectonic position, Fe, Ti, Al, and REE are the most reliable (Murray, 1994); (Ran et al., 2015). During diagenesis, SiO2 migrates; therefore, radiolarian tests are poorly preserved (Murray, 1994). This is the case in the present study; where the radiolarian tests are rarely identified in thin sections. Si/ (Si + Al + Fe + Ca) ratio (Table 1) is used to infer the source of silica, (Rangin et al., 1981); (Garbán et al., 2017). The high values of this ratio (between 0.8 and 0.9) indicate the predominantly biogenic origin of silica (Ruiz-Ortiz et al., 1989). The Si/ (Si + Al + Ca + Fe) value of Qulqula samples from the two sections is between 0.90 and 0.97, except for one sample with a low value (0.80). These high values clearly indicate the biogenic source of the silica. In addition, the negative correlation coefficient of SiO_2 with all other major oxides supports a biogenic source of silica. The presence of recrystallized radiolarian test in the Qulqula Formation indicates that these cherts derived from the diagenetic alteration of biogenic silica. However, contributions from other sources cannot be ruled out. The following equation is used to calculate the non-terrigenous fraction of SiO_2, (Wu et al., 2021):

$$SiO_2 non - terrigenous = SiO_2 bulk - (AlSi) terrigenous \times Al measured$$

$$Si\ non - ter = i\ -\ Al\ sample\ x \frac{i\ (\mathrm{PAAS})}{Al} \quad (1)$$

Where i: Represents concentration of the element. PAAS: Values from (McLennan, 2001). Si non-ter: Values of Qulqula Formation are between 97 – 100, except for two samples that have values of 94 and one sample has 83.

These values indicate that the majority of silica is of authigenic origin. On the other hand, the weak negative correlation between SiO_2 and CaO (r = - 0.18) indicates direct precipitation of silica from seawater and not diagenetic replacement of carbonate particles. The Mn-Fe-Al diagram is used for the classification of chert depositional environments, (Adachi et al., 1986). Due to the very low concentration of Mn, all analyzed samples were located along the Al-Fe line, and plotted in the non-hydrothermal chert field (Figure 16); supporting its biogenetic origin.

During the Early Cretaceous, the deep-water basin of the Qulqula Formation received silica from several sources. These silicas were precipitated commonly as the bedded sedimentary cherts and some of it as nodules, generally in a warm and arid paleoclimate, (Cecil & Edgar, 1994), and (Cecil & Edgar, 2003). The first source was the Mid-Oceanic Ridge with high quantities of silica released by submarine weathering (Figure 17). The second source was quartzose dust influx from the western desert as the primary source of silica. This condition is similar to the influx of silica-rich dust from the African Desert to the Amazon Forest, (Ben-Ami et al., 2010). The third source was a continental volcanic arc from which silica-rich mud reached the basin of QRF by turbidity current (Figure 17). The fourth source was radiolaria tests and sponges, whose siliceous remains are observed as a minor fraction of the silica in the bedded cherts. These sources supersaturated the environment QRF and developed bedded chert in deep basins below CCD where silica is stable instead of carbonates.

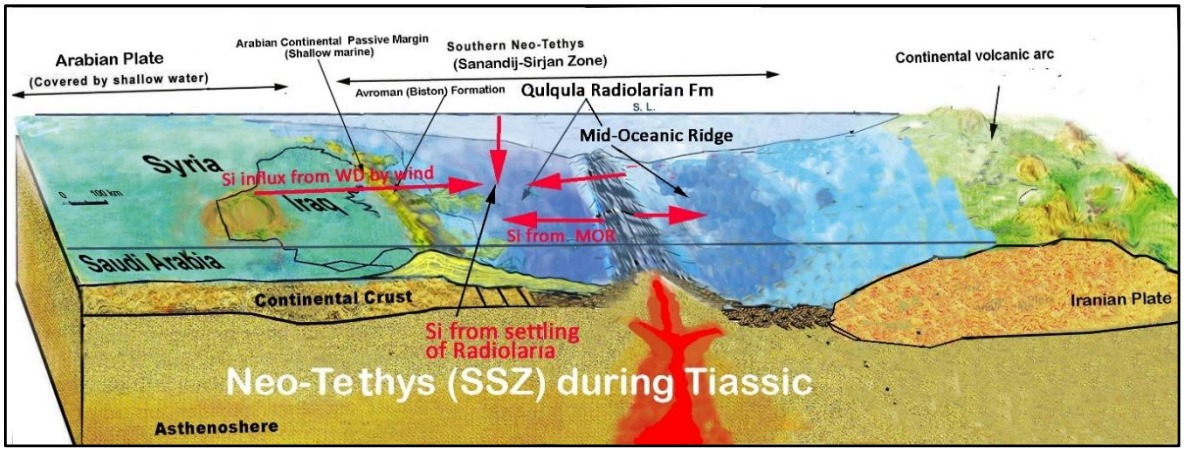

Figure 17. Neo-Tethys Sea during the Early Cretaceous in which the Qulqula Formation was deposited. Different inputs of silica can be observed from sources such as the Mid-Oceanic Ridge. Modified from (Mirza et al., 2021).

5.3. Redox conditions

Enrichment of some trace elements in sediments (such as V, U, and Mo) is related to the availability of oxygen in seawater, (Liu et al., 2019). V/(V+Ni) is widely used as an indicator for paleo-redox conditions. The high values (>0.82) may indicate euxinic conditions; 0.54 – 0.82, 0.46 – 0.60, and <0.46 indicate anoxic, dysoxic, and oxic conditions, respectively, (Hatch & Leventhal, 1992). The average V/ (V + Ni) values of the Qulqula Formation from the Zalan and Kaolose sections are 0.46 and 0.61, respectively (Table 2). These values indicate deposition under oxic-suboxic conditions. One sample from the lowermost part of the succession in the Kaolose section has a high value (0.8); indicating deposition under reducing-euxinic conditions. Under oxic conditions, the sediments are depleted with these elements; but under anoxic conditions; U, Th, and V become enriched and precipitated mainly as sulfide. Under euxinic conditions, Mo becomes also enriched. Therefore, the concentrations of these elements can be used as paleo-redox proxies (Chen et al., 2016). The enrichment factors of U and Th show low values; most of them are <1 (Table 2); suggesting deposition under oxic conditions. Again, the lowermost sample from the Kaolose section shows a high value; indicating deposition under reducing conditions. Oxic-dysoxic depositional environment is also supported by the inverse relationship between Ni/Co and V/Cr (Figure 18). One sample from the Kaolos section was suggested to be deposited under suboxic-anoxic conditions. This sample also has the highest Mo.

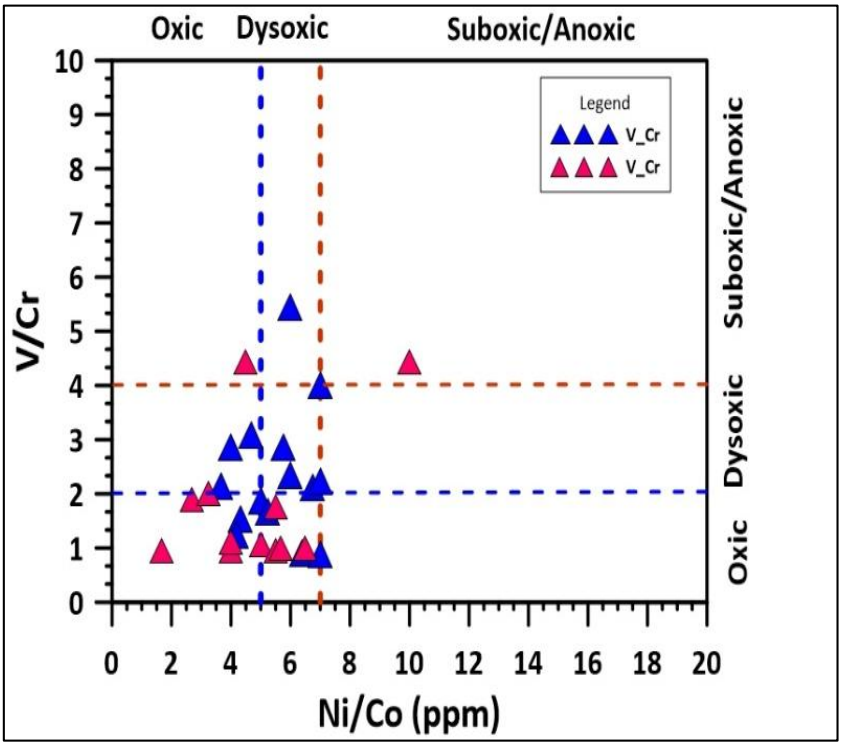

Figure 18. Ni/Co versus V/Cr redox index ((Hatch & Leventhal, 1992).

Mo is widely used as a redox proxy for bottom water due to its enrichment in organic-rich fine-grained sediments deposited under low oxygen conditions, (Tribovillard et al., 2006).

Generally, in sediments deposited under anoxic conditions Mo concentration is in the range of 2 – 25 ppm; whereas high concentrations (>100 ppm) indicate persistent euxinic conditions in unrestricted water (Scott & Lyons, 2012); (Gao et al., 2020). The studied samples of Qulqula Formation show slight, or no, Mo enrichment. Moreover, TOC-Mo covariation provides information about the degree of water restriction, (Algeo & Rowe, 2012a); (Zhu et al., 2022). In silled basins, Mo/TOC systematically decreases with increasing water restriction, (Algeo & Rowe, 2012b). In the present study samples; the Mo/TOC values are generally high (Table 2); they are in the range of 4.55 – 125, average 53 in the Zalan section; and 0.78 – 125, average 31 in the Kaolos section. These values are higher than that of the Black Sea, which is 4.5, (Algeo & Lyons, 2006); indicating deposition of the Qulqla Formation under open circulation marine conditions.

6. Conclusions

From the classification of siliciclastic sediment, these beds belong to the volcanic arc felsic rocks granite and diversional tectonic settings. High quantities of silica are released by submarine weathering of the Mid-Oceanic Ridge and quartzose dust influx from the western desert as the primary source of silica. Through the Mo/TOC relationship; it is evident that these chert beds are deposited under marine conditions. Trace element and ratio values indicate deposition under oxic-suboxic conditions and support the felsic provenance as well as Th-La-Sc and V-Ni-Th ternary diagrams. REE chondrite normalized shows that a little fractionation of plagioclase took place. The radiolaria tests and sponges, whose siliceous remains are observed as a minor fraction of the silica in the bedded cherts. These sources are supersaturated in the environment of QRF and developed bedded chert in deep basins below CCD where silica is stable instead of carbonates.

References

Adachi, M., Yamamoto, K., & Sugisaki, R. (1986). Hydrothermal chert and associated siliceous rocks from the northern Pacific their geological significance as indication of ocean ridge activity. *Sedimentary Geology*, *47*(1–2), 125–148.

Algeo, T. J., & Lyons, T. W. (2006). Mo–total organic carbon covariation in modern anoxic marine environments: Implications for analysis of paleoredox and paleohydrographic conditions. *Paleoceanography*, *21*(1).

Algeo, T. J., & Rowe, H. (2012a). Paleoceanographic applications of trace-metal concentration data. *Chemical Geology*, *324*, 6–18.

Algeo, T. J., & Rowe, H. (2012b). Paleoceanographic applications of trace-metal concentration data. *Chemical Geology*, *324*, 6–18.

Ali, S. A., Sleabi, R. S., Talabani, M. J. A., & Jones, B. G. (2017). Provenance of the Walash-Naopurdan back-arc–arc clastic sequences in the Iraqi Zagros Suture Zone. *Journal of African Earth Sciences*, *125*, 73–87.

Al-Maadhidi, A. S., Kadhim, L. S., & Alkhafaji, M. W. (2023). Trace and Rare Earth Elements Geochemistry of the Mudstone Rocks from the Injana Formation: Implications for Provenance and Paleoclimate. *The Iraqi Geological Journal*, 159–174.

Al-Qayim, B. A., Baziany, M. M., & Ameen, B. M. (2018). Mesozoic Tethyan Radiolarite age determination, Zagros suture zone, Kurdistan, NE Iraq. *The Iraqi Geological Journal*, 17–33.

Al-Qayim, B., Omer, A., & Koyi, H. (2012). Tectonostratigraphic overview of the Zagros suture zone, Kurdistan region, Northeast Iraq. *GeoArabia*, *17*(4), 109–156.

Al-Sheraefy, R. M., Ahmed, F. M., & Alrashedi, M. A. (2022). Geochemistry, Depositional Environment, and Provenance of the Cretaceous Radiolarian Chert in Northeastern Kurdistan, Iraq. *The Iraqi Geological Journal*, 43–59.

Altinli, I. E. (1966). Geology of Eastern and Southeastern Anatolia. *Bull. Min. Res. Explor. Inst.*, *60*.

Aswad, K. J., & Elias, E. M. (1988). Petrogenesis, geochemistry and metamorphism of spilitized subvolcanic rocks of the Mawat Ophiolite Complex, NE Iraq. *Ofioliti*, *13*(2/3), 95–109.

Baziany, M. M. (2014). *Depositional systems and sedimentary basin analysis of the Qulqula Radiolarian Formation of the Zagros Suture Zone*. https://www.researchgate.net/publication/262142815

Ben-Ami, Y., Koren, I., Rudich, Y., Artaxo, P., Martin, S. T., & Andreae, M. O. (2010). Transport of North African dust from the Bodélé depression to the Amazon Basin: a case study. *Atmospheric Chemistry and Physics*, *10*(16), 7533–7544.

Bolton, C. M. G., 1955b. (1955). *Report on the geology and economic prospect of the Qala Dizeh area Site*.

Buday, T. (1980). *The regional geology of Iraq: stratigraphy and paleogeography* (Vol. 1). State Organization for Minerals, Directorate General for Geological Survey ….

Cecil, C. B., & Edgar, N. T. (1994). *Predictive stratigraphic analysis: concept and application* (Issue 2110). US Government Printing Office.

Cecil, C. B., & Edgar, N. T. (2003). *Climate controls on stratigraphy*. SEPM Society for Sedimentary Geology.

Chen, C., Mu, C. L., Zhou, K. K., Liang, W., Ge, X. Y., Wang, X. P., Wang, Q. Y., & Zheng, B. S. (2016). The geochemical characteristics and factors controlling the organic matter accumulation of the Late Ordovician-Early Silurian black shale in the Upper Yangtze Basin, South China. *Marine and Petroleum Geology*, *76*, 159–175. https://doi.org/10.1016/J.MARPETGEO.2016.04.022

Cullers, R. L., & Graf, J. L. (1984). Rare earth elements in igneous rocks of the continental crust: intermediate and silicic rocks–ore petrogenesis. In *Developments in geochemistry* (Vol. 2, pp. 275–316). Elsevier.

Darvishzadeh, A. (1992). *Geology of Iran*. Neda publication.

Douville, E., Bienvenu, P., Charlou, J. L., Donval, J. P., Fouquet, Y., Appriou, P., & Gamo, T. (1999). Yttrium and rare earth elements in fluids from various deep-sea hydrothermal systems. *Geochimica et Cosmochimica Acta*, *63*(5), 627–643.

Evensen, N. M., Hamilton, P. J., & O'nions, R. K. (1978). Rare-earth abundances in chondritic meteorites. *Geochimica et Cosmochimica Acta*, *42*(8), 1199–1212.

Fu, X., Jian, W., Chen, W., Feng, X., Wang, D., Song, C., & Zeng, S. (2015). Organic accumulation in lacustrine rift basin: constraints from mineralogical and multiple geochemical proxies. *International Journal of Earth Sciences*, *104*, 495–511.

Gao, P., He, Z., Lash, G. G., Li, S., & Zhang, R. (2020). Origin of chert nodules in the Ediacaran Doushantuo Formation black shales from Yangtze Block, South China. *Marine and Petroleum Geology*, *114*, 104227.

Gao, P., He, Z., Lash, G. G., Zhou, Q., & Xiao, X. (2021). Controls on silica enrichment of lower Cambrian organic-rich shale deposits. *Marine and Petroleum Geology*, *130*, 105126.

Garbán, G., Martínez, M., Márquez, G., Rey, O., Escobar, M., & Esquinas, N. (2017). Geochemical signatures of bedded cherts of the upper La Luna Formation in Táchira State, western Venezuela: Assessing material provenance and paleodepositional setting. *Sedimentary Geology*, *347*, 130–147.

Ghafor, I. M., & Qadir, M. M. (2009). Larger foraminifera (Alveolinidae, Soritidae, and Nummulitidae) from the Former Qulqula Conglomerate Formation, Kurdistan Region, Northeastern Iraq. *Iraqi Journal of Earth Sciences*, *9*(1), 35–54.

Hatch, J. R., & Leventhal, J. S. (1992). Relationship between inferred redox potential of the depositional environment and geochemistry of the Upper Pennsylvanian (Missourian) Stark Shale Member of the Dennis Limestone, Wabaunsee County, Kansas, USA. *Chemical Geology*, *99*(1–3), 65–82.

Jassim, S. Z., & Goff, J. C. (2006). *Geology of Iraq*. DOLIN, sro, distributed by Geological Society of London.

Karim H. K. (2024). Karim, K. H. (2024) Problems of the Zagros Ophiolites and Basaltic Bodies, Examples from Kurdistan Region, Northern Iraq, Inżynieria Mineralna, Vol.1, no.1, http://doi.org/10.29227/IM-2024-01-18. *Inżynieria Mineralna, Vol.1*, *No.1*, *1*(1).

Karim, K. H., & Abioui, M. (2023). Significance of the lithic volcanic detritus and crystalloclasts in development of paleogeography of the Zagros collisional belt: evidence from the Kurdistan Region, Northeastern Iraq. *Journal of Sedimentary Environments*, *8*(1), 23–38.

Karim, K. H., & Baziany, M. M. (2007). Relationship between Qulqula conglomerate formation and red bed series, at Qulqula area, NE-Iraq. *Iraqi Journal of Earth Sciences*, *7*(1), 1–12.

Karim, K. H., Habib, H. R., & Raza, S. M. (2009). Lithology of the lower part of Qulqula Radiolarian Formation (Early Cretaceous), Kurdistan Region, NE Iraq. *Iraqi Bulletin of Geology and Mining*, *5*(1), 9–23.

Kato, Y., & Nakamura, K. (2003). Origin and global tectonic significance of Early Archean cherts from the Marble Bar greenstone belt, Pilbara Craton, Western Australia. *Precambrian Research*, *125*(3–4), 191–243.

LaGrange, M. T., Konhauser, K. O., Catuneanu, O., Harris, B. S., Playter, T. L., & Gingras, M. K. (2020). Sequence stratigraphy in organic-rich marine mudstone successions using chemostratigraphic datasets. *Earth-Science Reviews*, *203*, 103137.

Lawa, F. A., Koyi, H., & Ibrahim, A. (2013). Tectono-stratigraphic evolution of the NW segment OF the Zagros fold-thrust belt, Kurdistan, NE Iraq. *Journal of Petroleum Geology*, *36*(1), 75–96.

Liu, W., Yao, J., Tong, J., Qiao, Y., & Chen, Y. (2019). Organic matter accumulation on the Dalong Formation (Upper Permian) in western Hubei, South China: Constraints from multiple geochemical proxies and pyrite morphology. *Palaeogeography, Palaeoclimatology, Palaeoecology*, *514*, 677–689.

Ma, P., Wang, L., Wang, C., Wu, X., & Wei, Y. (2015). Organic-matter accumulation of the lacustrine Lunpola oil shale, central Tibetan Plateau: Controlled by the paleoclimate, provenance, and drainage system. *International Journal of Coal Geology*, *147*, 58–70.

Mateen, A., Wahid, A., Janjuhah, H. T., Mughal, M. S., Ali, S. H., Siddiqui, N. A., Shafique, M. A., Koumoutsakou, O., & Kontakiotis, G. (2022). Petrographic and Geochemical Analysis of Indus Sediments: Implications for Placer Gold Deposits, Peshawar Basin, NW Himalaya, Pakistan. *Minerals*, *12*(8). https://doi.org/10.3390/min12081059

McLennan, S. M. (2001). Relationships between the trace element composition of sedimentary rocks and upper continental crust. *Geochemistry, Geophysics, Geosystems*, *2*(4).

McLennan, S. M., Hemming, S., McDaniel, D. K., & Hanson, G. N. (1993). *Geochemical approaches to sedimentation, provenance, and tectonics*.

McLennan, S. M., Taylor, S. R., McCulloch, M. T., & Maynard, J. B. (1990). Geochemical and Nd Sr isotopic composition of deep-sea turbidites: crustal evolution and plate tectonic associations. *Geochimica et Cosmochimica Acta*, *54*(7), 2015–2050.

Mirza, T. A., Karim, K. H., Ridha, S. M., & Fatah, C. M. (2021). Major, trace, rare earth element, and stable isotope analyses of the Triassic carbonates along the northeastern Arabian Plate margin: a key to understanding paleotectonics and paleoenvironment of the Avroman (Biston) limestone formation from Kurdistan region, northeastern Iraq. *Carbonates and Evaporites*, *36*(4), 66.

Murray, R. W. (1994). Chemical criteria to identify the depositional environment of chert: general principles and applications. *Sedimentary Geology*, *90*(3–4), 213–232.

Omar, A. A., Lawa, F. A., & Sulaiman, S. H. (2015). Tectonostratigraphic and structural imprints from balanced sections across the north-western Zagros fold-thrust belt, Kurdistan region, NE Iraq. *Arabian Journal of Geosciences*, *8*, 8107–8129.

Owen, A. W., Armstrong, H. A., & Floyd, J. D. (1999). Rare earth elements in chert clasts as provenance indicators in the Ordovician and Silurian of the Southern Uplands of Scotland. *Sedimentary Geology*, *124*(1–4), 185–195.

Pearce, J. A., Harris, N. B. W., & Tindle, A. G. (1984). Trace element discrimination diagrams for the tectonic interpretation of granitic rocks. *Journal of Petrology*, *25*(4), 956–983.

Ran, B., Liu, S., Jansa, L., Sun, W., Yang, D., Ye, Y., Wang, S., Luo, C., Zhang, X., & Zhang, C. (2015). Origin of the Upper Ordovician–lower Silurian cherts of the Yangtze block, South China, and their palaeogeographic significance. *Journal of Asian Earth Sciences*, *108*, 1–17.

Rangin, C., Steinberg, M., & Bonnot-Courtois, C. (1981). Geochemistry of the Mesozoic bedded cherts of Central Baja California (Vizcaino-Cedros-San Benito): implications for paleogeographic reconstruction of an old oceanic basin. *Earth and Planetary Science Letters*, *54*(2), 313–322.

Ruiz-Ortiz, P., Bustillo, M., Molina, M., & Al, A. (1989). *Radiolarite Sequences of the Subbetic, Betic Cordillera, Southern Spain*.

Scott, C., & Lyons, T. W. (2012). Contrasting molybdenum cycling and isotopic properties in euxinic versus non-euxinic sediments and sedimentary rocks: Refining the paleoproxies. *Chemical Geology*, *324*, 19–27.

Sissakian, V. K., & Fouad, S. F. (2014). Geological map of Sulaimaniyah Quadrangle, scale 1: 250000. *Iraq Geological Survey Publications, Baghdad, Iraq.*

Tatzel, M., von Blanckenburg, F., Oelze, M., Bouchez, J., & Hippler, D. (2017). Late Neoproterozoic seawater oxygenation by siliceous sponges. *Nature Communications*, *8*(1), 621.

Taylor, S. R., & McLennan, S. M. (1985). *The continental crust: its composition and evolution*.

Tribovillard, N., Algeo, T. J., Lyons, T., & Riboulleau, A. (2006). Trace metals as paleoredox and paleoproductivity proxies: an update. *Chemical Geology*, *232*(1–2), 12–32.

Wu, W., Liu, W., Mou, C., Liu, H., Qiao, Y., Pan, J., Ning, S., Zhang, X., Yao, J., & Liu, J. (2021). Organic-rich siliceous rocks in the upper Permian Dalong Formation (NW middle Yangtze): Provenance, paleoclimate and paleoenvironment. *Marine and Petroleum Geology*, *123*, 104728.

Zhu, B., Yang, T., Wang, J., Chen, X., Pan, W., & Chen, Y. (2022). Multiple controls on the paleoenvironment of the early Cambrian black shale-chert in the northwest Tarim Basin, NW China: Trace element, iron speciation, and Mo isotopic evidence. *Marine and Petroleum Geology*, *136*, 105434.

About the author

Dr. Sardar M. Ridha is an assistant professor at the University of Sulaimaniyah, College of Sciences, Dept. of Earth Sciences and Petroleum. He is a member of the Kurdistan Geological Society and the Union of Iraqi Geologists. He got an M.Sc. in hydrogeochemistry/from the University of Baghdad and a Ph.D. in sedimentary geochemistry/University of Sulaimani. He has 12 years of experience in the oil fields as a wellsite geologist starting from SOC in Basrah (North Rumaila, West Qurma, Zubir, and Safwan oil fields for 7 years) and also as a senior wellsite geologist with (DNO, GasPlus, and DanaGas companies) in (Tawki, Benenan, Shewashan and Kormore fields) for 4 years separately.

e-mail: sardar.ridha@univsul.edu.iq